Supporting Information

Lau and Kim 10.1073/pnas.1418682112

SI Text

Model Experiment and Background

CMIP5 is the latest model intercomparison project sponsored by the World Climate Research Program's Working Group on Coupled Modeling to provide a framework for coordinated climate change experiments. The scope of CMIP5 include long-term simulations with different concentration pathways of emission mitigation scenarios, near-term decadal simulations, and emission-driven Earth System Model experiments (1, 2). The 1% per year CO_2 emission increase scenario used for this study applies to a suite of experiments designed to provide a calibration of the model's internal climate variability and response to increasing CO_2 (2). Experiments were started from the preindustrial levels of CO_2 concentration achieving a quadrupling of CO_2 at the end of a 140-y simulation. For this work, we used 33 participating models with various horizontal resolutions, ranging from 0.75° to 3.75°. Monthly mean winds, vertical motion, and precipitation data are regridded to a common grid (2.5° by 2.5°). CMIP5 model outputs are available from Earth System Grid Federation (ESGF) gateways (Program for Climate Model Diagnosis and Intercomparison, British Atmospheric Data Center, Deutsches Klimarechenzentrum, and National Computational Infrastructure), and links to ESGF gateways and modeling centers are available from cmip-pcmdi.llnl.gov/cmip5/availability.html.

Vertical Motions

Changes in the rising branch of the HC, as reflected by the 500-hPa pressure velocity averaged over different latitudinal width, are shown in Fig. S1. In the near-equatorial regions (5°S–5°N), there is a robust increasing trend in upward motion, as indicated by the near-constant positive slope ($\sim 5.2 \pm 1.0\%\ K^{-1}$) and the small spread among the models. At wider latitude bands (10°S–10°N and 20°S–20°N), the changes in vertical motions are substantially muted. When the zonal averages are taken over the entire tropics (30°S–30°N), the vertical motions again show a robust rise, but with much smaller amplitude compared with 5°S–5°N. Based on the signs of the control and the trends, these results indicate that global warming enhances mean rising motion over the entire tropics (30°S–30°N), with the strongest signal coming from the near-equatorial region (5°S–5°N).

Monthly Outgoing Longwave Radiation and Daily Cloud-Top Temperature

Monthly outgoing long wave radiation (OLR) is used as a proxy for tropical convection in this study. To better interpret the physical meaning of OLR with respect to tropical convection, we have investigated the relationship between observed OLR from National Oceanic and Atmospheric Administration Advanced Very High Resolution Radiometer (3) and daily Visible and Infrared Scanner Channel-4 brightness temperature T_b from Tropical Rainfall Measuring Mission. Fig. S2 shows the pdfs of daily T_b corresponding to different bands of OLR, i.e., OLR $< 220\ W{\cdot}m^{-2}$ (band 1), $220\ W{\cdot}m^{-2} <$ OLR $< 270\ W{\cdot}m^{-2}$ (band 2), and OLR $> 270\ W{\cdot}m^{-2}$ (band 3) used in *Tropical Convection* to describe the physical nature of the cloud system. Here, daily values of $T_b = 273$ K will be identified as the mean freezing level of the standard tropical atmosphere. The pdfs indicate that the three OLR bands are contributed by distinctly different cloud systems as evident in the wide range of T_b distributions with respect to the freezing level. Based on the fraction (α) of the daily population with $T_b < 273$ K, band 1 ($\alpha = 71\%$), band 2($\alpha = 25\%$), and band 3 ($\alpha = 3\%$) can be interpreted, respectively, as contributions from mostly of ice-phase deep clouds, mixed-phase middle clouds, and warm shallow clouds.

Anomalous Meridional Wind Height–Latitude Cross Sections of Individual Models

Fig. S3 shows the robustness of the response in the meridional wind as indicated by almost all models showing qualitatively the same response, i.e., a characteristic quadruple pattern in the upper troposphere (<300 hPa), signaling a rise of the region of maximum outflow of the HC, and a somewhat weakened return flow in the lower troposphere (>800 hPa) and near the surface toward the equator.

Time Variation of Meridional Wind Profile

The time evolution of the meridional wind anomaly at 10°N and 10°S, respectively (Fig. S4), shows an increasingly stronger (weaker) outflow above (below) 200 hPa, in both hemispheres, as the CO_2 concentration increases. The near-constant positive slopes of the total wind isotachs above 200 hPa reflect a steady rise (~3.5 hPa per decade) of the region of maximum outflow of the HC. Computations of the meridional mass flux, i.e., mass weighted meridional wind at different cross sections show that the mass outflow at the upper portion (200–100 hPa) out of the 10°S–10°N zone is intensifying at a fast rate of $+9.8 \pm 0.7\%\ K^{-1}$. The rate of increase is even faster at $+17.0 \pm 1.7\%\ K^{-1}$, out of the 5°S–5°N zone, which corresponds to the core ascending branch of the HC. The increased meridional mass flux is compensated by strong inflow in the lower portion (400–200 hPa) of the climatological outflow region. Even with the strong compensation, the net anomalous mass flux over the climatological outflow region (400–100 hPa) out of the 5°S–5°N zone is still increasing, albeit at a much reduced net rate of $1.9 \pm 0.8\%\ K^{-1}$.

Meridional Mass Streamfunction and Zonal Wind

Changes in the HC associated with the DTS and their connection to the global circulations can also be clearly seen in the anomalous meridional mass streamfunction and zonal winds (Fig. S5). From the signs and locations of the anomalies compared with the control (Fig. S5*A*), it is clear that the upper branches (above 250 hPa) of the HC in the deep tropics are strengthened, while the lower portion (1,000–300 hPa) is weakened, consistent with an elevation of the climatological region of maximum outflow, i.e., a rise of the center of mass of the HC. The rise together with enhanced upper tropospheric vertical motion associated with DTS in the ascending branch of the HC allow stronger poleward outflow in the upper troposphere, thus extending the subsidence branches of the HC in both hemispheres further poleward from their climatological positions. A similar polar extension of the Ferrel cells in both hemispheres, although with much smaller amplitude, can also be discerned. The rise of the center of maximum outflow in the upper branch of the HC is also reflected in changes in the structure of the zonal wind anomaly (Fig. S5*B*). The most pronounced zonal wind acceleration is found near 100 hPa, above the climatological center at 150–200 hPa in both hemispheres. The subtropical westerly acceleration in both hemispheres is likely to be driven by the deeper convection, and the Coriolis force from the stronger outflow in the upper troposphere associated with the meridional wind anomalies noted in Fig. 3*A* and Fig. S3. Previous studies have suggested that the extratropical maximum may be related to enhanced baroclinicity due to increased temperature gradient at the upper troposphere, and polar shift of the wintertime storm tracks (4, 5).

Latitude–Height Cross Sections of Moisture Convergence

The DTS is associated with strong moisture convergence in the lower troposphere in the near-equatorial region, and with moisture divergence in an expanded subtropical divergence region from 10 to 50 latitude in both hemisphere (Fig. S6). The moisture convergence increases RH in the lower to middle troposphere of the deep tropics, and the moisture divergence leads to the RH deficit in the troposphere. As explained *in Meridional Outflow and Relative Humidity*, the RH anomaly pattern is a function of both dynamics and thermodynamics, i.e., more water vapor under warmer conditions, and different dynamical feedbacks in the ascending and descending branches of the HC.

Decomposition of Precipitation Anomalies

The decomposition of total precipitation into evaporation, advection, dynamic convergence, and transients is based on Eq. **1**. Comparing the change pattern and magnitude with the total precipitation change (Fig. S7*A*), it can be seen that evaporation increases over the ocean almost everywhere, except in the North Atlantic and part of the Southern Ocean, but reduces over land regions in the subtropics, i.e., southern Europe, northern Africa, South Africa, and the tropics, i.e., the Maritime continent, southern Australia, southwest United States/Mexico, and Amazonia. However, evaporation contributes little to the structure change of the precipitation, i.e., the DTS and drying of the subtropics. Advection ($-V \cdot \nabla q$) contributes strongly to the RH deficit over the west coast of North America, northern South America, northeast Africa, northern India, and northeastern East Asia and moderately to the drying of the oceanic regions adjacent to the DTS, but not much to the DTS itself (Fig. S7*C*). The combined effect of negative moisture advection and reduced evaporation over tropical and subtropical land regions is consistent with the increased GDI over these regions (Fig. 5*A*), stemming from strong atmosphere–land surface feedback. Clearly, from Fig. S7 *A* and *D*, dynamic convergence ($-\mathrm{q}\ \nabla \cdot \mathbf{V}$) is the major contributor to the structural change of precipitation over the oceanic regions of the tropics and the subtropics, including the DTS, and strong drying in adjacent regions, and broader subtropical regions of the HC. In the equatorial Pacific region, the contribution can be more than 90% of the total precipitation change.

Temperature and Moisture Response

Under a 1% per year increase in CO_2 emission, the MMM atmosphere warms by longwave absorption throughout the troposphere up to the tropopause, while the lower stratosphere and regions above cool from reduced longwave radiation from below (Fig. S8). The warming is rather nonuniform. In the tropics, the warming of the upper troposphere is much (>8 °C) stronger than that in lower troposphere (~1–2 °C) because warm air tends to rise following the moist adiabatic lapse rate. At higher latitudes, the warming is mostly confined to the surface and lower troposphere. Tropospheric moisture is increased everywhere following the Clausius–Clapeyron law governing saturated water vapor and temperature, with the largest increase in the tropics. However, because of the rapid decrease of moisture with height, the rate of increase of water vapor in the upper troposphere cannot keep up with the accelerated increase in temperature there. As a result, an RH deficit develops in the upper and middle troposphere under global warming. The pattern of RH deficit is further modified by subsidence anomalies associated with changes in the HC as discussed in Fig. 4.

Anomaly Patterns of Relative Humidity in the Middle and Lower Troposphere

At 500 hPa and at 850 hPa (Fig. S9 *A* and *B*), the RH pattern is almost identical to the respective regression pattern with DTS upper troposphere outflow (Fig. 4 *A* and *B*). Key features at 500 hPa include (*i*) increased RH associated with DTS along the equator, with the most prominent signal over the central and eastern equatorial Pacific, (*ii*) moderate reduction in RH in the eastern equatorial Indian Ocean and western Maritime continent, Mexico, and Amazonia, and (*iii*) prevailing reduction of RH over the rest of the globe, with the strongest signal at the polar flank of the subtropical dry zones. At 850 hPa, the RH pattern shows similar characteristics from *i* to *iii*, but with more regionalized features, including strong reduction over land regions of southern Europe and North Africa, South Africa, western Australia, and southern Chile. Other regions with large RH deficit include tropical regions of southwestern United States and Mexico, and Amazonia. These regions coincide well with regionals of large rainfall deficit, expanded descending branch of the HC (Fig. 4*C*), and region of maximum GDI (Fig. 5*A*).

1. Meehl GA, Bony S (2011) Introduction to CMIP5. *CLIVAR Exchanges Newsl* 16(2):4–5.
2. Taylor KE, Stouffer RJ, Meehl GA (2012) An overview of CMIP5 and the experiment design. *Bull Am Meteorol Soc* 93:485–498.
3. Liebmann B, Smith CA (1996) Description of a complete (interpolated) outgoing longwave radiation dataset. *Bull Am Meteorol Soc* 77:1275–1277.
4. Lu J, Chen G, Frierson DMW (2008) Response of the zonal mean atmospheric circulation to El Niño versus global warming. *J Clim* 21:5835–5851.
5. Kushner PJ, Held IM, Delworth TL (2001) Southern Hemisphere atmospheric circulation response to global warming. *J Clim* 14:2238–2249.

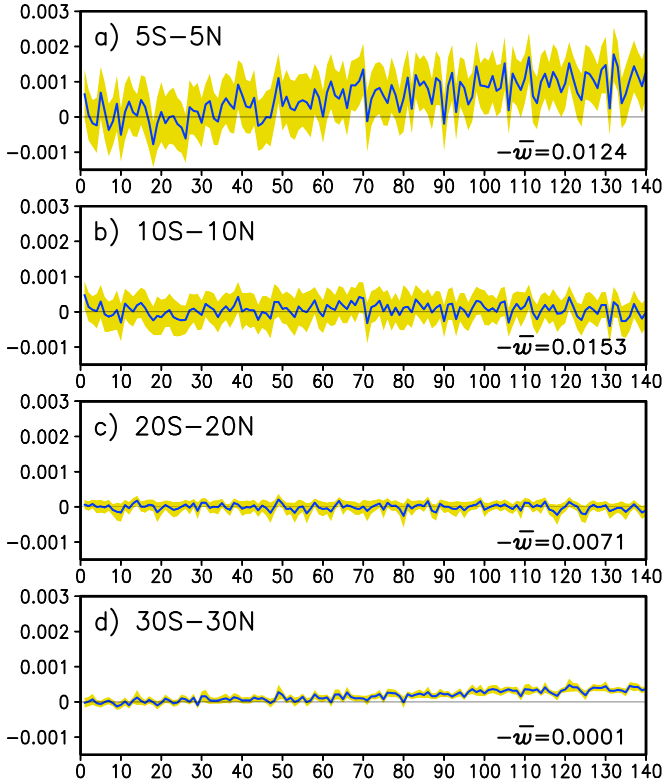

Fig. S1. Time series of 140 simulated years of MMM 500-hPa vertical motion averaged between (*A*) 5°S and 5°N, (*B*)10°S and 10°N, (*C*) 20°S and 20°N, and (*D*) 30°S and 30°N, under 1% per year increase CO_2 emission scenario. The MMM is computed from 33 CMIP5 models, and the model spread (yellow shading) is the SE of the MMM. Unit is negative pascals per second. The number in the lower right-hand corner indicates the MMM vertical velocity in the control.

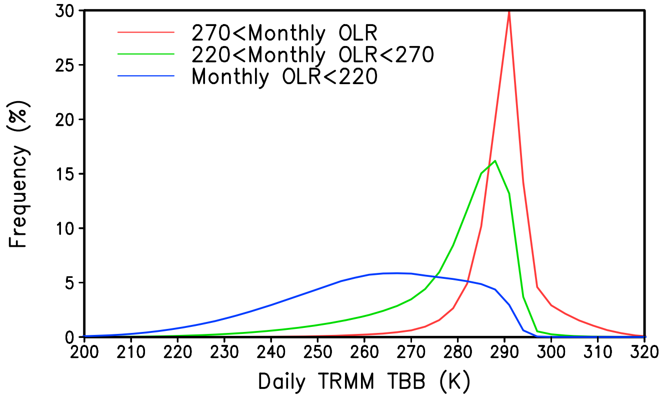

Fig. S2. Probability distribution functions of daily T_b for three different monthly OLR bands over the tropics (30°S–30°N) for the period 1998–2012.

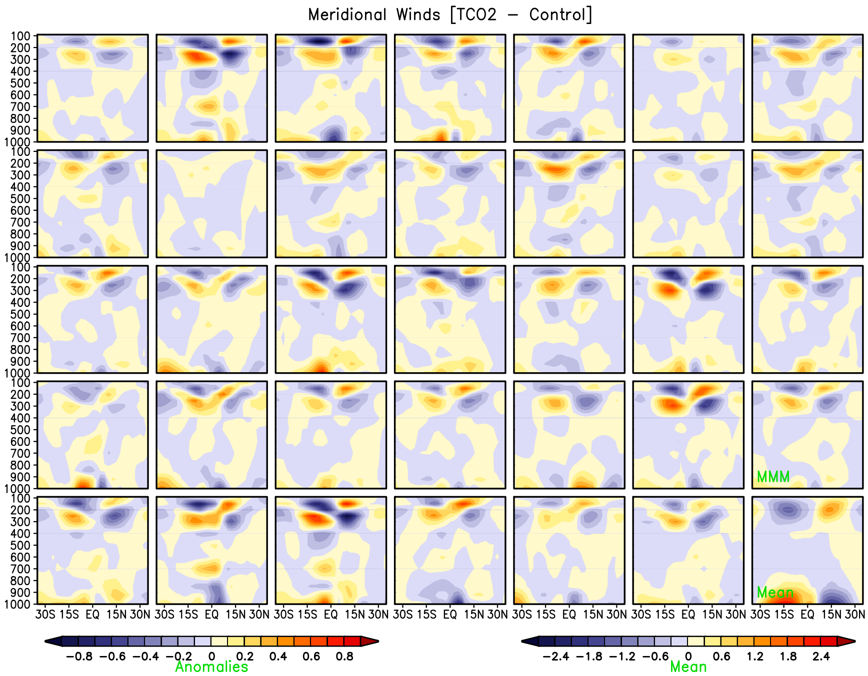

Fig. S3. Latitude–height cross sections of anomalous meridional winds in the tropics for each of 33 CMIP5 models. The MMM anomaly and control are shown in the bottom two panels of the last column. Unit is meters per second.

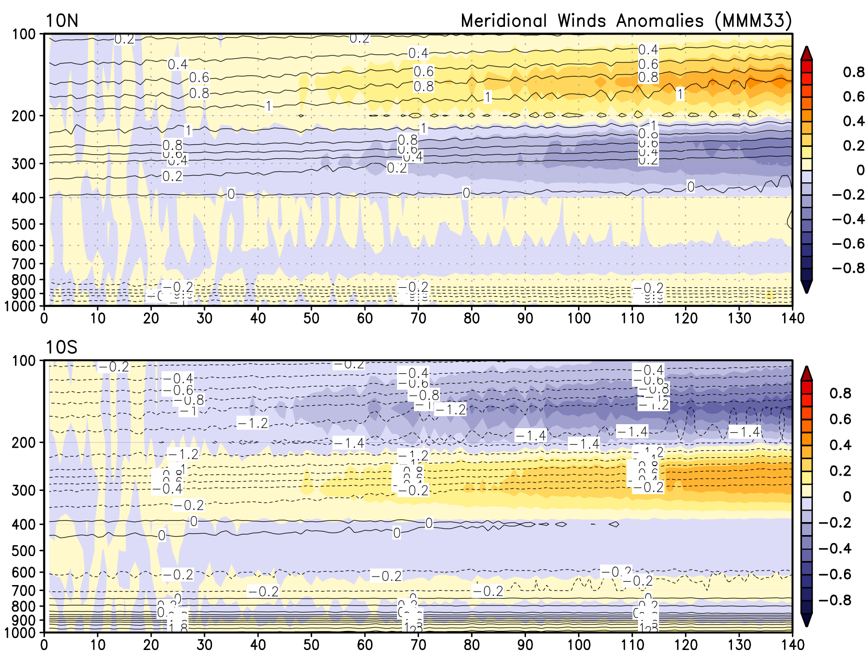

Fig. S4. Time–height cross section of meridional winds at 10°N (*Upper*) and 10°S (*Lower*). Unit is meters per second.

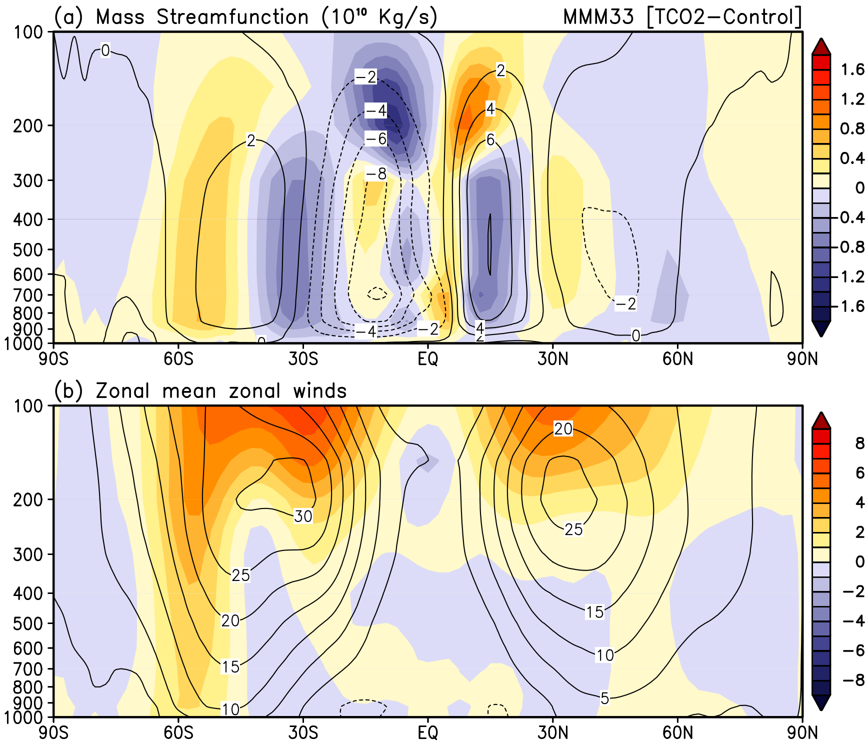

Fig. S5. MMM climatology (contour) and anomalies (colored) for (*A*) meridional mass streamfunction and (*B*) zonal mean winds. Unit of mass streamfunction is 10^{10} kg·s^{-1}, and zonal wind is meters per second.

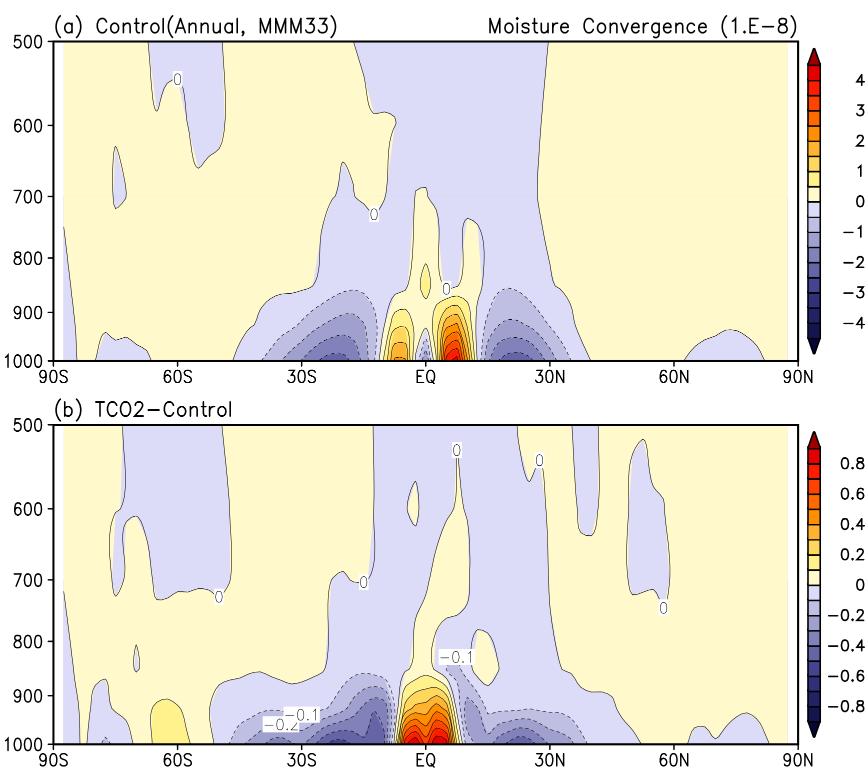

Fig. S6. Latitude–height cross section of MMM horizontal moisture convergence for (*A*) climatology and (*B*) anomaly. Unit is 10^{-8} g·kg^{-1}·s^{-1}.

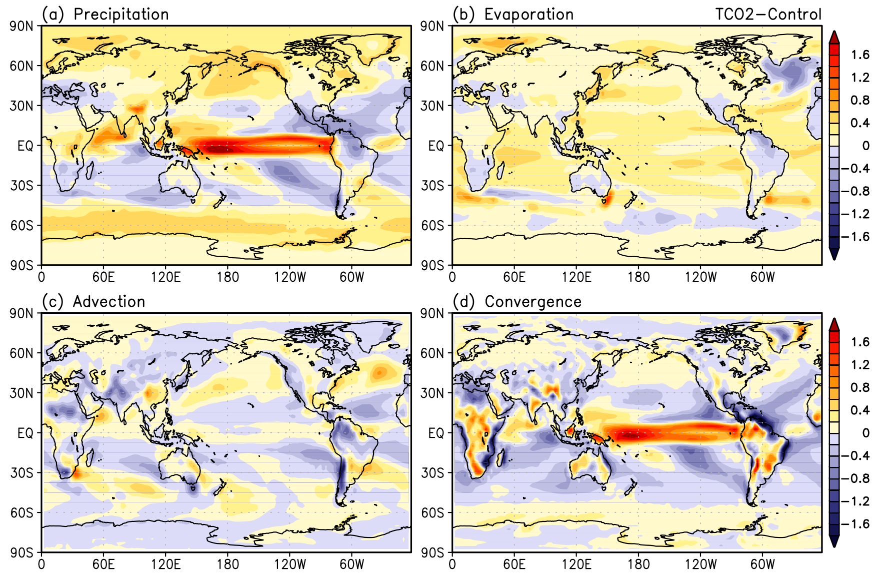

Fig. S7. Anomaly patterns of (*A*) total rainfall, and contributions from (*B*) evaporation, (*C*) advection, and (*D*) dynamic convergence. See *Merdional Outflow and Relative Humidity* for explanation. Unit is millimeters per day.

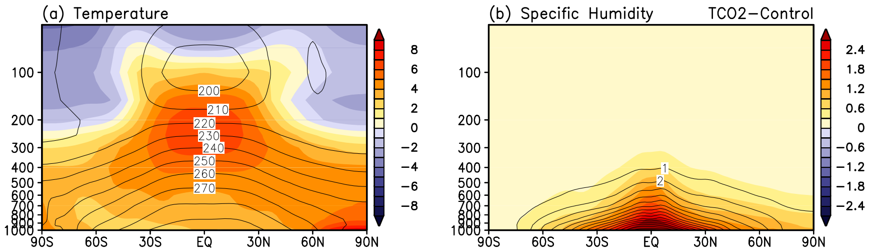

Fig. S8. Latitude–height cross section of MMM climatology (contour) and anomalies (color) for (*A*) temperature (per degree kelvin) and (*B*) specific humidity (grams per kilogram).

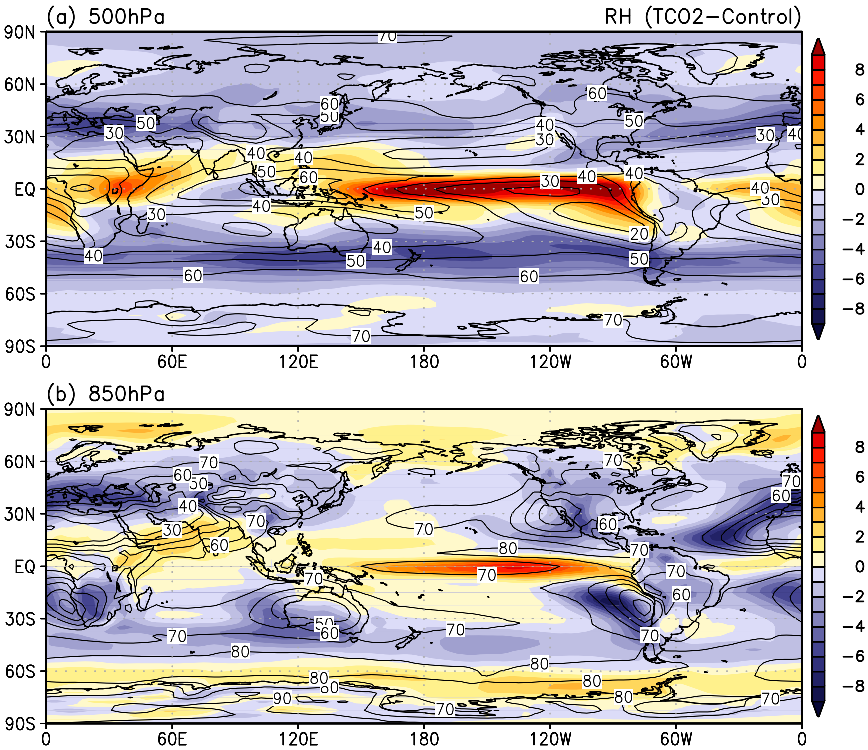

Fig. S9. Anomaly RH patterns at (*A*) 500 hPa and (*B*) 850 hPa, under global warming. Units are in percentage. Climatology is in contour, and anomaly is in color.